Enhancement of Flame Retardant Performance of Bio-Based Polylactic Acid Composites with the Incorporation of Aluminum Hypophosphite and Expanded Graphite

Gang Tang [a b] , Rui Zhang [c] , Xin Wang [a] , Bibo Wang [a] , Lei Song [a] , Yuan Hu [a b] & Xinglong Gong [a d]

[a] State Key Laboratory of Fire Science, University of Science and Technology of China, Hefei, Anhui, P. R. China

[b] Suzhou Key Laboratory of Urban Public Safety, Suzhou Institute for Advanced Study, University of Science and Technology of China, Suzhou, Jiangsu, P. R. China

[c] College of Chemical Engineering, Nanjing Forestry University, Nanjing, Jiangsu, P. R. China

[d] CAS Key Laboratory of Mechanical Behavior and Design of Materials, Department of Modern Mechanics, University of Science and Technology of China, Hefei, Anhui, P. R. China

PLEASE SCROLL DOWN FOR ARTICLE

Taylor & Francis
Taylor & Francis Group

Enhancement of Flame Retardant Performance of Bio-Based Polylactic Acid Composites with the Incorporation of Aluminum Hypophosphite and Expanded Graphite

GANG TANG[1,2], RUI ZHANG[3], XIN WANG[1], BIBO WANG[1], LEI SONG[1], YUAN HU[1,2*], and XINGLONG GONG[1,4]

[1]*State Key Laboratory of Fire Science, University of Science and Technology of China, Hefei, Anhui, P. R. China*
[2]*Suzhou Key Laboratory of Urban Public Safety, Suzhou Institute for Advanced Study, University of Science and Technology of China, Suzhou, Jiangsu, P. R. China*
[3]*College of Chemical Engineering, Nanjing Forestry University, Nanjing, Jiangsu, P. R. China*
[4]*CAS Key Laboratory of Mechanical Behavior and Design of Materials, Department of Modern Mechanics, University of Science and Technology of China, Hefei, Anhui, P. R. China*

A series of flame retarding biodegradable polylactic acid composites (FR-PLA) based on aluminum hypophosphite (AHP) and expanded graphite (EG) were prepared by the melt-compounding method. The effect of AHP and EG on the flame retardancy and thermal stability of PLA were investigated by thermogravimetric analysis (TGA), UL-94 vertical burning test, limiting oxygen index, microscale combustion calorimetry and cone calorimeter testing. The gas products of PLA and FR-PLA composites were investigated by TG-IR technology. TGA results showed that the FR-PLA composites presented higher char residue and reduced mass loss rate than neat PLA. Significant improvement of flame retardancy of PLA/AHP/EG composites indicated an excellent synergistic effect between AHP and EG. Cone calorimeter tests gave clear evidence that the combination of AHP and EG resulted in a significant reduction of the heat release rate (HRR) and total heat release (THR). TG-IR revealed that the combination of AHP and EG resulted in significant decrease of gas products. The char residue of FR-PLA composites were also investigated by scanning electron microscope, Fourier transform infrared spectra spectroscopy and X-ray photoelectron spectroscopy. Based on the analysis, possible flame retardant mechanism was discussed.

Keywords: Polylactic acid, flame retardant, aluminum hypophosphite, expanded graphite, polymer-matrix composites

1 Introduction

In recent years, increasing awareness of the limited petroleum resource and the environmental burden caused by the persistent plastic wastes have led to extensive research aimed at developing eco-friendly and renewable polymers to replace traditional petroleum-based plastics (1–3). Among these biodegradable polymers, polylactic acid (PLA) has received increasing attention because of its biodegradable, abundant renewable source, transparency and excellent mechanical properties. Due to its excellent properties, PLA has various applications, such as automotive components, electrical industry, building materials, and the aerospace industry (4–7). However, poor fire resistance of PLA (typical limiting oxygen index of 19.5, easy dripping in burning) restricts its application in some fields like electronic appliances where high flame retardancy is required. Therefore, the modification for flame retardant PLA is still an important and urgent task.

However, only a few studies on the flame retardancy of PLA has been done up to now. Several researchers employed ammonium phosphate (8, 9), aluminium hydroxide (10) melamine phosphate (11), silica gel (12) and compounds containing halogen and talc (13) as additives for flame retardant in PLA matrix. Aluminum hypophosphite (AHP) is an excellent halogen free flame retardant which is widely used for many engineering plastics, such as PET, PBT and PA (14–16). However, few research reports have been focused on flame retarded PLA with AHP.

*Address correspondence to: Yuan Hu, State Key Laboratory of Fire Science, University of Science and Technology of China, 96 Jinzhai Road, Hefei, Anhui 230026, P. R. Chin and Suzhou Key Laboratory of Urban Public Safety, Suzhou Institute for Advanced Study, University of Science and Technology of China, 166 Ren'ai Road, Suzhou, Jiangsu 215123, P. R. China. Fax/Tel: +86-551-3601664; Email: yuanhu@ustc.edu.cn

Expanded graphite (EG) is an intrinsical graphite inserted by sulfuric acid or nitric acid between the graphite layers. In recent years, polymer composites reinforced by expanded graphite have shown substantial improvements in mechanical properties, thermal conductivity, electrical conductivity and barrier properties in several polymers, such as, PE (17), PS (18), EVA (19), PMMA (20), phenolic resin (21) and so on. Expanded graphite is also well known as a typical intumescent flame retardant and suppressor for smoke (22–24). When EG is exposed to heat, it could expand and generate a voluminous insulative layer thus providing fire-retardant performance to the polymeric matrix (25). Recently, many literatures have reported the research of flame-retardant polymer treated with EG (26–29). Porous foamed carbonaceous layer is formed during the burning process of polymer/EG composites, which could act as a barrier to interrupt the combustion. However, the porous foamed carbonaceous mass is so loose that it has poor mechanical properties and often exfoliates from the matrix, resulting in an incomplete protective char layer. Therefore, it is meaningful to generate a compact char structure to improve the flame retardant properties of polymer/EG composites. In the present work, aluminum hypophosphite in combination with expanded graphite was added into polylactic acid to prepare flame retardant polymer materials. The thermal, flame retardancy and mechanical properties of PLA composites were investigated by thermal gravimetric analysis (TGA), limiting oxygen index (LOI), UL-94 vertical burning test, microscale combustion calorimetry (MCC), and cone calorimeter test (CCT). The gas production of FR-PLA composites were investigated by TG-IR. In addition, the char residues after cone testing were investigated by scanning electron microscope (SEM) Fourier transform infrared spectra spectroscopy (FTIR) and X-ray photoelectron spectroscopy (XPS). Furthermore, possible flame retardant mechanism was also discussed.

2 Experimental

2.1 Materials

PLA resin (Nature Works 4032D) in granular form was supplied by Cargill Dow Inc. (America). Aluminum hypophosphite (AHP) was supplied by Hanye chemical New Material Co., Ltd (China). Expanded graphite (EG) was supplied by Qingdao Tianhe Graphite Co., Ltd (China).

2.2 Preparation of FR-PLA Composites

PLA resin, AHP and EG were dried at 80°C overnight before used. All the samples were prepared by a twin-roll mixing mill (XK-160, Jiangsu, China) at 175°C and the rotation speed of screw was 100 rpm. PLA was first added to the mill at the beginning of the blending procedure. After PLA was molten, the additives were then added to the matrix and processed about 10 min until a visually good dispersion was achieved. The mixtures after mixing processing were cut into pellets and then hot-pressed into sheets under 10 MPa for 10 min. The sheets were cut into suitably sized specimens for fire testing. The detailed formulations of the samples are shown in Table 1. In Table1, the digital represents weight percent of the additives in the composites. For example, PLA/20AHP contains 20 wt% of AHP and 80 wt% PLA. To further investigate the effect of AHP to EG on the flame retardancy of the composites, composites mixtures with various ratios of AHP and EG at the additives at 20 wt% were prepared. In PLA/10AHP/10EG, it contains 10 wt% of AHP, 10 wt% EG and 80 wt% of PLA.

2.3 Measurement and Characterization

2.3.1 *Morphology and Dispersibility*

The morphology of the sample after being gold-sputtered (EG, AHP particles and FR-PLA composites) were studied

Table 1. Results of LOI and UL-94 tests for neat PLA and FR-PLA composites

| | Composition (wt%) | | | | UL-94 | | |
Sample	PLA	AHP	EG	LOI	$t_1/t_2{}^a$ (s)	dripping	Rating
PLA	100	0	0	19.5	BC[b]	Y	NR[c]
PLA/10AHP	90	10	0	25.5	10.7/1.7	Y	V2
PLA/15AHP	85	15	0	27.5	8.3/3.4	Y	V2
PLA/20AHP	80	20	0	28.5	0.9/5.8	N	V0
PLA/10EG	90	0	10	28.5	BC	Y	NR
PLA/15EG	85	0	15	36	10.8/2.2	Y	V2
PLA/20EG	80	0	20	41	1.8/8.1	Y	V1
PLA/15AHP/5EG	80	15	5	31	0.9/1.1	N	V0
PLA/10AHP/10EG	80	10	10	34	1.0/2.2	N	V0
PLA/5AHP/15EG	80	5	15	43	1.4/4.7	Y	V1

[a]t_1 and t_2, average combustion times after the first and the second applications of the flame;
[b]BC, burns to clamp;
[c]NR, not rated.

by a PHILIPS XL30E scanning electron microscope. The FR-PLA composites were cryogenically fractured in liquid nitrogen and then sputter-coated with a conductive layer. The accelerated voltage was 20 KV.

2.3.2 *Thermogravimetric Analysis*

Thermal gravimetric analysis (TGA) was performed using a Q5000 IR (TA Instruments) thermo-analyzer instrument under nitrogen and air conditions. Samples were measured in an alumina crucible with a mass of about 5–10 mg. Composites in an open Pt pan were tested at temperature ranging from room temperature to 800°C with a heating rate of 20°C/min.

2.3.3 *Limiting Oxygen Index*

LOI tests were measured according to ASTM D2863 by HC-2 oxygen index meter (Jiangning Analysis Instrument Company, China). The specimens used for the test were of the dimensions of $100 \times 6.5 \times 3$ mm^3.

2.3.4 *UL94 Vertical Burning Tests*

UL-94 vertical burning tests were performed using vertical burning instrument (CFZ-2-type, Jiangning Analysis Instrument Company, China) with plastic samples of dimensions $130 \times 13 \times 3$ mm^3, suspended vertically above a cotton patch. The classifications are defined according to the American National Standard UL-94.

2.3.5 *Microscale Combustion Calorimetry*

Microscale combustion calorimetry (MCC, Govmark) was used to analyze combustion properties of the samples according to ASTM D 7309-7. 4–6 mg samples were heated to 650°C at a heating rate of 1°C/s in a stream of nitrogen flowing at 80 cm^3/min. The volatile anaerobic thermal degradation products in the nitrogen gas stream were mixed with a 20 cm^3/min stream of pure oxygen prior to entering a 900°C combustion furnace. The heat release rate (HRR) in watts per gram of sample (W/g) was calculated from the oxygen depletion measurements. The total heat release (THR) in kJ/g was obtained by integrating the HRR curve.

2.3.6 *Cone Calorimetry*

Cone calorimeter combustion tests were performed on the cone calorimeter (Fire Testing Technology, UK) according to ISO5660 standard procedures, each sample with dimension $100 \times 100 \times 3$ mm^3 was wrapped in an aluminum foil and exposed horizontally to 35 kW/m^2 external heat flux.

2.3.7 *Thermogravimetric Analysis-infrared Spectrometry*

TG-IR was performed using the TGA Q500 thermogravimetric analyzer (TA Instruments) that was linked to the Nicolet 6700 FTIR spectrophotometer. About 10–15 mg of the sample was put in an alumina crucible and heated from 30 to 700°C. The heating rate was 20°C/min in nitrogen atmosphere with flow rate of 70 ml/min.

2.3.8 *Residue Analysis*

Some residues of the samples after cone testing were collected and further analyzed by scanning electron microscope (SEM). The SEM micrographs were obtained with a scanning electron microscope PHILIPS XL30E at an accelerating voltage of 20 kV. The specimens were sputter-coated with a conductive layer.

Fourier transform infrared spectra spectroscopy (Nicolet 6700 FT-IR spectrophotometer) was employed to characterize the residues collected after Cone calorimeter tests using thin KBr disc. The transition mode was used and the wavenumber range was set from 400 to 4000 cm^{-1}.

X-ray photoelectron spectroscopy (XPS) was used to analyze the residue char after Cone calorimeter test, and it was carried out with a VG Escalab Mark II spectrometer (Thermo-VG Scientific Ltd.), using Al Ka excitation radiation (hν = 1253.6 eV).

3 Results and Discussion

3.1 Morphology and Dispersibility

Figure 1 shows SEM images of AHP and EG particles. Figure 1(a) presents AHP particles with a low magnification; it is interesting to find that AHP has a wide particle size distribution from 0.1 μm to 20 μm. Figure 1(b) shows AHP particles with a high magnification, from which we can find some AHP particles have an irregular surface, which may come from the processing technology. Figures 1(c) and (d) show EG particles with a low magnification and high magnification, respectively. It can be seen from the images that,
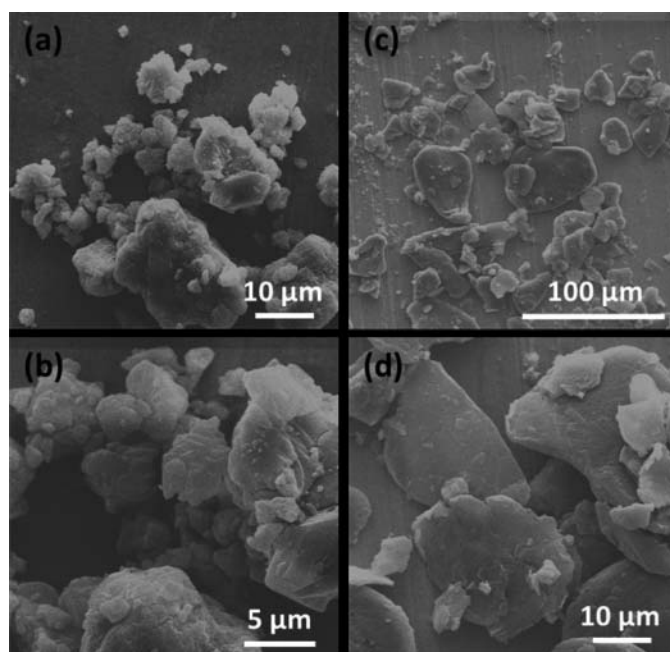

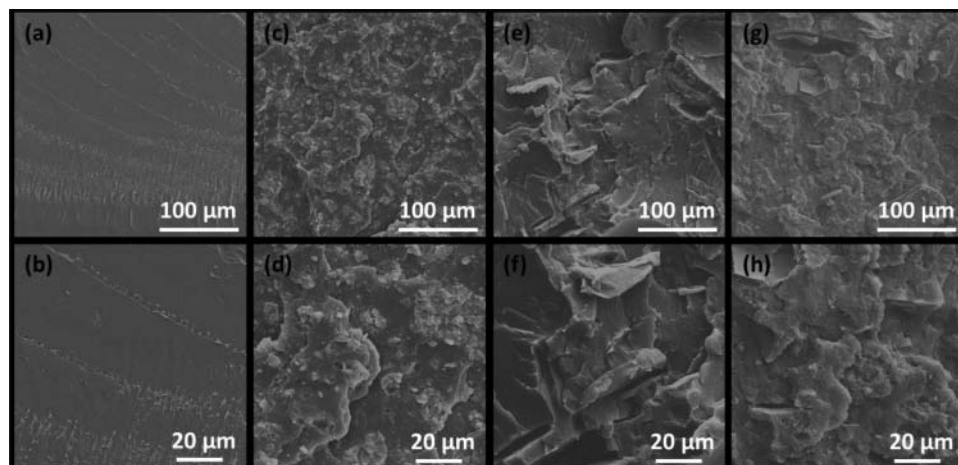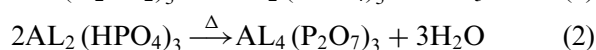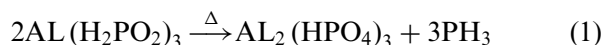**Fig. 1.** SEM image of AHP and EG particle: AHP (a, b); EG (c, d).

Fig. 2. SEM image of PLA (a, b), PLA/20AHP (c, d), PLA/20EG (e, f) and PLA/10AHP/10EG (g, h).

EG presents a lamellar structure with a wide particle size distribution of 1 μm-50 μm.

To further investigate the dispersion of the additives in PLA matrix, SEM was carried out and the corresponding results are shown in Figure 2. Figures 2(a) and (b) show the fractured surface of PLA, which presents a smooth surface. Figures 2(c) and (d) show the fracture of PLA/20AHP at low and high magnification, which present a fine dispersion of AHP particles in PLA/20AHP. Figures 2(e) and (f) are the SEM images of PLA/20EG, and the EG particles are uniformly dispersed in PLA. The surface becomes mat with some holes on it, which may be explained by that the EG particles are huge and present poor compatibility with PLA matrix. Figures 2(g) and (h) are the fracture of PLA/10AHP/10EG, from which we can see that AHP and EG particles are homogenously dispersed.

3.2 Thermal Stability of PLA and FR-PLA Composites

The TG and DTG curves of AHP and EG in nitrogen are shown in Figure 3, and the corresponding data are listed in Table 2. The onset degradation temperature of samples was evaluated by the temperature of 5 wt% weight loss ($T_{-5\%}$); T_{max} is defined as the temperature at which the samples process the maximal mass loss rate (MMLR). EG starts to decompose at 259°C, and the thermal degradation process only has one stage. The stage is in the range of 250–350°C, corresponding to a DTG peak at 256°C, and the char residue of EG at 800°C is about 78.1%. The thermal decomposition of AHP can be divided into two stages corresponding to T_{max} at 351°C and 434°C, respectively. The decomposition process of AHP could be represented by the two equations as detailed below:

$$2AL(H_2PO_2)_3 \xrightarrow{\Delta} AL_2(HPO_4)_3 + 3PH_3 \quad (1)$$

$$2AL_2(HPO_4)_3 \xrightarrow{\Delta} AL_4(P_2O_7)_3 + 3H_2O \quad (2)$$

The typical TG and DTG traces for PLA and FR-PLA composites under nitrogen atmosphere are given in Figure 4. Pure PLA shows the onset decomposition temperature ($T_{-5\%}$) is at 353°C, and the thermal decomposition process only has one stage with a T_{max} at 392°C. Pure PLA leaves almost no char residue at 800°C.

For FR-PLA composites containing AHP, the decomposition process of PLA/10AHP and PLA/20AHP also exhibits two stages. The first stage can be attributed to the decomposition of AHP, while the second one corresponds to the decomposition of PLA matrix. However, the decomposition temperature of PLA/20AHP is lower than pure PLA, which may result from the poor thermal stability of AHP. PLA/10AHP and PLA/20AHP present the char residue of 7.3 wt% and 14.6 wt%, respectively, indicating that the addition of AHP increases the thermal stability of PLA/AHP composites at high temperature (>450°C).
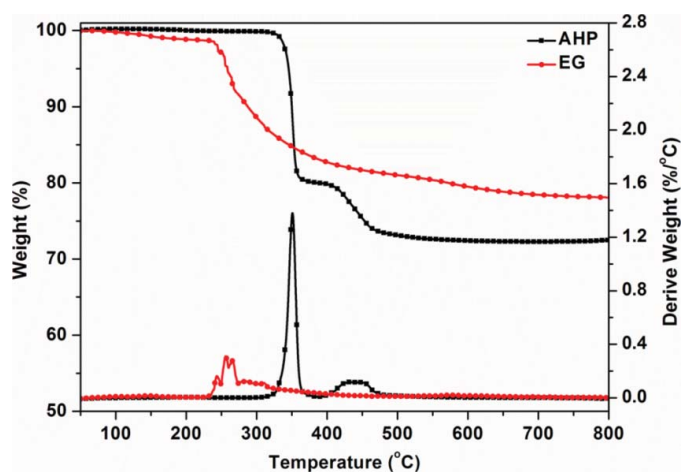

Fig. 3. TGA and DTG curves of AHP and EG under nitrogen conditions. (Color figure available online.)

Table 2. TG and DTG data of PLA, EG, AHP and FR-PLA composites under nitrogen condition

Sample	$T_{-5\%}$ (°C)	T_{max1} (°C)	MMLR1[a] (%/°C)	T_{max2} (°C)	MMLR2 (%/°C)	Residues[b] (wt%)
PLA	353	—	—	392	2.90	0.2
EG	259	256	0.31	—	—	78.1
AHP	346	351	1.38	434	0.12	72.5
PLA/10AHP	353	351	0.48	394	2.69	7.3
PLA/20AHP	348	350	0.63	394	2.24	14.6
PLA/10EG	359	—	—	395	2.67	10.3
PLA/20EG	347	—	—	393	2.16	16.1
PLA/15AHP/5EG	347	347	0.47	393	2.21	16.2
PLA/10AHP/10EG	351	350	0.33	396	2.25	15.4

[a]Maximal mass loss rate.
[b]At 800°C.

For FR-PLA composites containing EG, the decomposition process of PLA/10EG and PLA/20EG present one stage which corresponds to the decomposition of PLA. The onset decomposition temperatures are 359°C and 347°C for PLA/10EG and PLA/20EG, respectively.

PLA/15AHP/5EG shows an onset decomposition temperature at 347°C. It is interesting to find that the T_{max} at the first stage of PLA/15AHP/5EG is 3°C lower compared with PLA/20AHP, which may be caused by the intercalation agents in EG (such as H_2SO_4 and HNO_3) promote the degradation of AHP. However, for all of the FR-PLA composites, the addition of AHP and EG results in a slight increase the second maximal mass loss rate, indicating the additives inhibit the degradation of PLA at high temperature.

The decomposition behaviors of PLA, EG and FR-PLA composites are further investigated by Thermal gravimetric analysis in air condition. The TG and DTG curves are shown in Figure 5, and the corresponding data are presented in Table 3. It is interesting to find that the TG curve of EG shows two decomposition stage compared to that in nitrogen. The first stage in the range of 230–300°C corre-

sponds to the degradation of intercalation agent and the second stage between 650°C and 800°C indicates the oxidation of char. The char residue at 800°C is 9.4%. which is much less than that in nitrogen condition. For FR-PLA composites containing EG, PLA/10EG and PLA/20EG show two stage decomposition, the first stage at the range of 320–400°C is due to the decomposition of PLA matrix, and the second stage from 700°C to 800°C indicates the oxidation process of char layer. For FR-PLA composites containing AHP, both PLA/10AHP and PLA/20AHP present a high char residue compared with those in nitrogen, which is due to the oxidation process of low valence of phosphorus. When combined AHP with EG, PLA/15AHP/5EG shows one stage decomposition without the visible oxidation process of char layer, indicating that AHP can promote the formation of a more stable char layer in air condition.

3.3 LOI and UL-94 Tests

The LOI values and UL-94 results of FR-PLA composites are shown in Table 1. Pure PLA is highly combustible with a low LOI value of 19.5%, and it shows no rating in the
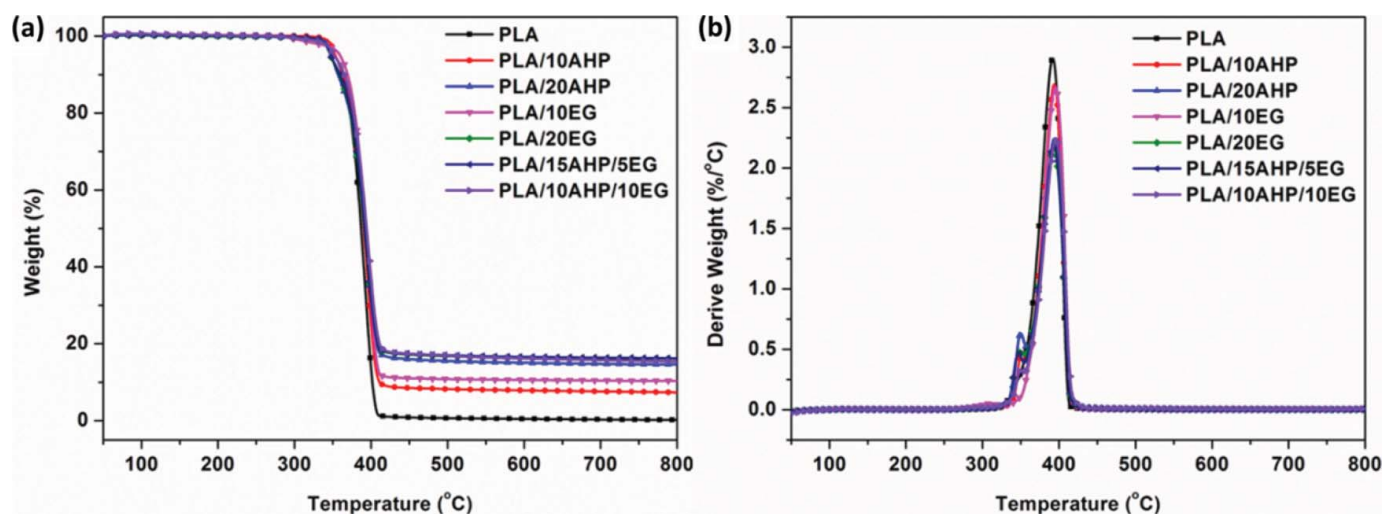

Fig. 4. TGA and DTG curves of PLA and FR-PLA composites under nitrogen conditions. (Color figure available online.)

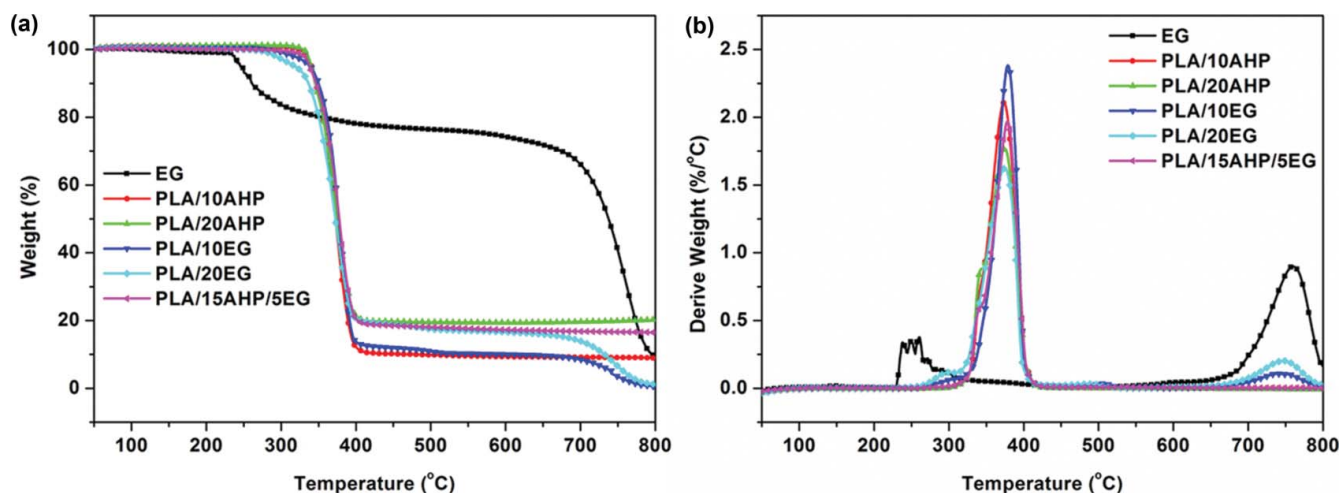**Table 3.** TG and DTG data of EG and FR-PLA composites under air conditions

Sample	$T_{-5\%}$ (°C)	T_{max1} (°C)	MMLR1 [a] (%/°C)	T_{max2} (°C)	MMLR2 (%/°C)	Residues [b] (wt%)
EG	245	260	0.38	760	0.90	9.4
PLA/10AHP	340	373	2.11	—	—	8.9
PLA/20AHP	340	375	1.77	—	—	20.2
PLA/10EG	339	379	2.38	744	0.11	0.6
PLA/20EG	319	374	1.62	747	0.20	1.1
PLA/15AHP/5EG	338	378	1.97	—	—	16.5

[a]Maximal mass loss rate.
[b]At 800°C.

Table 4. Data recorded in MCC measurement

Specimen	HRC (J/g*K)	pHRR (W/g)	THR (KJ/g)	T_{PHRR} (°C)
PLA	382	390	14.2	390
PLA/10AHP	346	346	12.6	392
PLA/20AHP	296	298	12	392
PLA/10EG	362	362	12	386
PLA/20EG	294	296	11.1	379
PLA/15AHP/5EG	288	290	12	392
PLA/10AHP/10EG	300	302	11.6	388
PLA/5AHP/15EG	284	285	11.2	386

HRC: heat release capacity, ±5J/g*K; pHRR: peak of release rate, ±5 W/g; THR: total heat release, ±0.1 KJ/g; T_{PHRR}: temperature at PHRR, ±2°C.

Table 5. Combustion parameters obtained from cone calorimeter

Sample	TTI (s)	Tp (s)	pHRR (kW/m²)	THR (MJ/m²)	FPI	FGI
PLA	57	155	549	62.2	0.10	3.5
PLA/10AHP	45	115	368	60.2	0.12	3.2
PLA/20AHP	41	95	285	57.7	0.14	3.0
PLA/10EG	46	75	244	60.2	0.19	3.3
PLA/20EG	46	95	356	43.5	0.13	3.7
PLA/15AHP/5EG	54	80	260	49.8	0.21	3.2

TTI: time to ignition, ±2 s; pHRR: peak heat release rate, ±15 kW/m²; T_P: time to pHRR, ±2 s; THR: total heat release, ±0.5 MJ/m².

Fig. 5. TGA and DTG curves of EG and FR-PLA composites under air conditions. (Color figure available online.)

UL-94 test. The incorporation of AHP results in a significant increase in LOI value but only shows a UL-94 V-2 rating. When the AHP content was increased to 20 wt%, the PLA/20AHP sample displays a LOI value of 28.5%, and can meet V-0 rating in the UL-94 testing. The addition of EG has a significantly positive effect on the LOI value of FR-PLA, but shows poor performance in UL-94 testing. When AHP is combined with EG, PLA/15AHP/5EG and PLA/10AHP/10EG can meet UL-94 V-0 rating, with a higher LOI value of 31% and 34 %, respectively. Further increasing the EG content results in poor performance in UL-94 testing for PLA/5AHP/15EG, but an amazing high LOI value. From the above result, it can be concluded that EG is an effective carbonization agent for PLA, and the combination of EG and AHP could promote the formation of protective char layer, so the flame retardancy of PLA composites are significantly increased.

3.4 Microscale Combustion Calorimeter

Microsale combustion Calorimeter (MCC) measures the flammability of materials on milligram quantities, which is based on the principle of oxygen consumption to measure the rate and amount of heat during combustion (30). In the measurement of MCC, the heat is generated by fully combustion of the fuel gases produced during the pyrolysis of samples. Several parameters can be obtained from MCC, such as heat release rate (HRR), heat release capacity (HRC), total heat release (THR), etc., which are very important to reflect the combustion properties of materials, allowing a reasonable estimation of fire hazard using small quantities of samples.

The HRR curves of PLA and FR-PLA are shown in Figure 6, and the corresponding data are displayed in Table 4. As for virgin PLA, the pHRR value of PLA is 390 W/g,
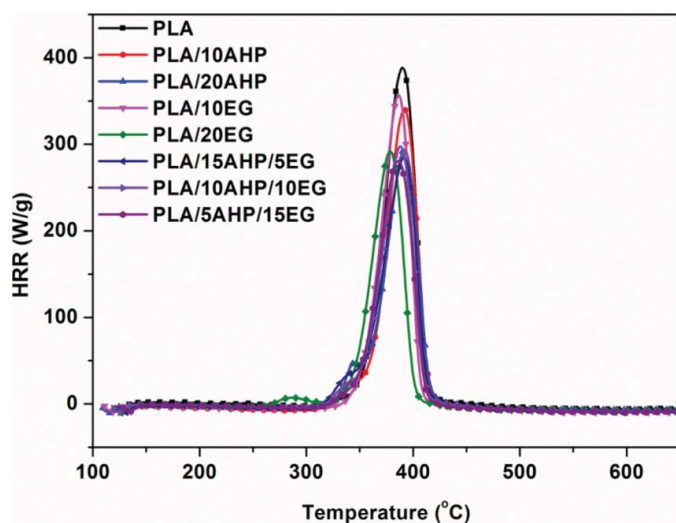
while that of PLA/10AHP, PLA/20AHP, PLA/10EG and PLA/20EG is 346 W/g, 298 W/g, 362 W/g, 296 W/g, respectively. The sample PLA/15AHP/5EG, which contains AHP and EG simultaneously, exhibits the lowest pHRR value of 290 W/g, corresponding to a 25.6% reduction compared with that of pure PLA. THR, calculated from the total area under the HRR peaks, is another important parameter used to evaluate fire hazard. The PLA/10AHP, PLA/20AHP, PLA/10EG and PLA/20EG exhibit THR values of 12.6 kJ/g, 12.0 kJ/g, 12.0 kJ/g and 11.1 kJ/g, respectively, which are 11.3%, 15.5%, 15.5% and 21.8% reduction compared to pure PLA. PLA/15AHP/5EG shows THR of 12.0 kJ/g, a 15.5% reduction compared to pure PLA.

Moreover, the incorporation of AHP content results in a slight increase of the temperature at pHRR, whereas the EG addition reduces this value. This can be explained by the fact that the degradation of AHP induces the formation of thermally stable aluminium phosphate and aluminium pyrophosphate, which functions as a barrier to hinder the degradation of PLA, while the acid species in EG promote the degradation of PLA, thus result in the decrease of temperature at pHRR.

3.5 Cone Calorimeter Test

As is well known, cone calorimeter is a useful bench-scale test for simulating real-world fire conditions (31). In this study, cone calorimeter test was used to further investigate the influence of AHP and EG on the flammability of FR-PLA composites during the combustion process; the detailed data are showed in Table 5. Figure 7 shows the heat release rate (HRR) curves of PLA, PLA/AHP, PLA/EG and PLA/AHP/EG composites. It can be seen that pure PLA burns fast after ignition and a sharp HRR peak
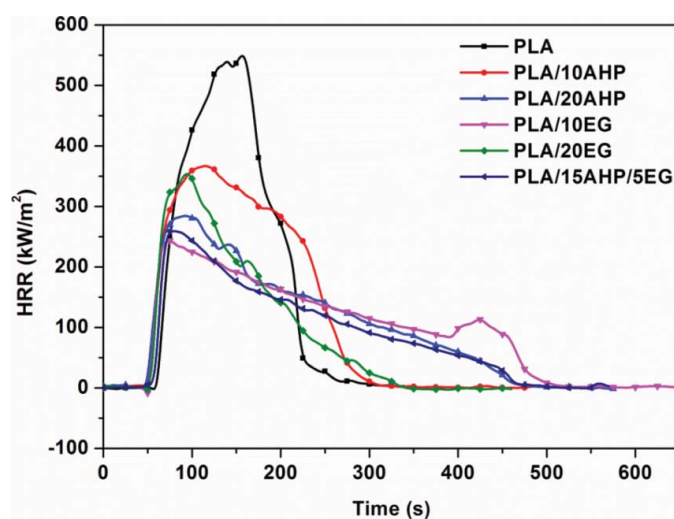

Fig. 6. Heat release rate curves of PLA and FR-PLA composites from the MCC test. (Color figure available online.)

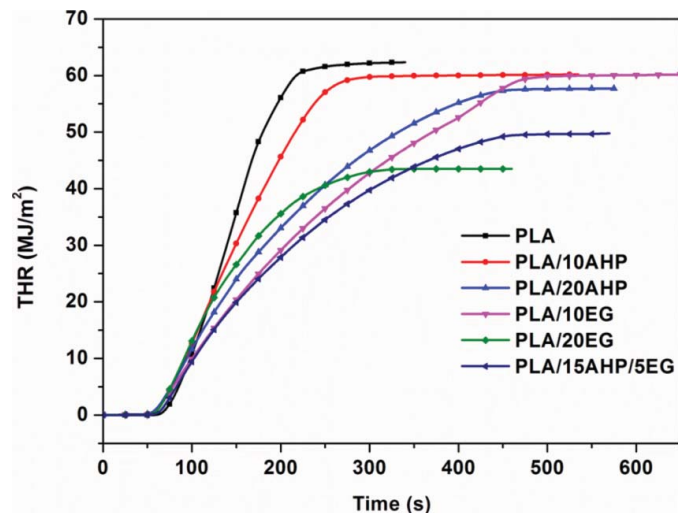**Fig. 7.** Heat release rate curves for samples from cone calorimeter test. (Color figure available online.)

Fig. 8. Total heat release curves for samples from cone calorimeter test. (Color figure available online.)

appears with a pHRR value of 549 kW/m^2. For FR-PLA composites containing 10 wt% and 20 wt% of AHP, the pHRR values are reduced to 368 and 285 kW/m^2, respectively. The pHRR value of FR-PLA composites containing 10 wt% EG is decreased to 244 kW/m^2. However, the pHRR value is increased to 356 kW/m^2 with the further increase of EG content. Maintaining the content of the flame retardant at 20 wt%, the combination of AHP and EG significantly decrease the pHRR value to 260 kW/m^2, with a reduction of 52.3% compared to pure PLA.

Figure 8 shows the total heat release (THR) curves of PLA, PLA/AHP, PLA/EG and PLA/AHP/EG composites. At the end of the burning, pure PLA releases a total heat of 62.3 KJ/m^2. The addition of AHP content slight change THR values for PLA/AHP composites. This may because that PH$_3$ generate in the degradation process of AHP, which could act as fuel and consume a lot of oxygen. Compared to pure PLA, THR values of PLA/10EG and PLA/20EG composites are 60.2 and 43.5 KJ/m^2, respectively. The composites PLA/15AHP/5EG shows THR value of 49.8 KJ/m^2. Although the TTI values of FR-PLA composites are decreased by the incorporation of the AHP or EG, the increasing TTI value results from the composites containing AHP and EG shows the highest TTI value, indicating better fire retardancy property.

Fire propagation index (FPI) and fire growth index (FGI) are introduced to comprehensively investigate the fire safety properties of the materials. FPI is defined as the ratio of time to ignition (TTI) and peak heat release rate (pHRR), indicating the difficult degree flashover of material after it is ignited. The larger the value of FPI, the lower hazard of the material. FGI is defined as the ratio of peak heat release rate (pHRR) and time to peak heat release rate (Tp), which reflects the spread speed of the fire. The larger the value of FGI, the higher hazard of the material. From Table 5, it is

obvious to find that the addition of AHP and EG results in a significant increase in FPI values and the reduction in FGI value, indicating lower fire hazard for FR-PLA composites compared with neat PLA. It is interesting to find that PLA/15AHP/5EG composite shows the highest FPI values, proving the existence of synergistic effect between AHP and EG in FR-PLA composites.

Photographs of the residues after the cone calorimeter test are shown in Figure 9. As can be observed, there is almost no residue after burning for pure PLA. The residue of PLA/20AHP (Fig. 9b) displays an un-intumescent but compact char layer. Figure 9(c) shows the residue of PLA/20EG, which presents a significant intumescent but almost collapsed layer. The residue of PLA/15AHP/5EG, as shown in Figure 9(d) shows a compact and intumescent char layer, suggesting that the combination of AHP and EG results in a strong and compact char, which could be the reason for obtaining better flame retardancy for PLA/AHP/EG composite.

3.6 Decomposition Products

3D TG-IR spectra for the thermal decomposition of PLA and FR-PLA composites are shown in Fig. 10. The peaks of around 3500–3600, 2700–3000, 2100–2400, 1300–1450, 1100–1200 cm^{-1} are noted. Some of the gaseous decomposition products of PLA are unambiguously identified by characteristic FTIR signals, such as water (3575 cm^{-1}) compounds containing carbonyl group (1760 cm^{-1}) and methyl-substituted compounds (3000 cm^{-1}) (32).

In order to clearly understand the change of these volatilized products, major signals from the gas-phase spectra changing with time are separated from the 3D spectra. The spectra are shown in Figure 11. The main products of the thermal decomposition of PLA are compounds containing OH (such as H$_2$O, 3400–3600 cm^{-1}), CO$_2$ (2360 cm^{-1}), aliphatic ethers (1120 cm^{-1}), hydrocarbons (C-H stretching at 1373 cm^{-1}), compounds containing carbonyl group (1760 cm^{-1}), etc (33–35). As shown in Figure 11(a), CO$_2$ is detected at 18.2 min, but the signal is weak. At 19.2 min, water (3575 cm^{-1}), methyl-substituted compounds (3000 cm^{-1}), CO$_2$ (2360 cm^{-1}), CO (2180, 2110 cm^{-1}), compounds containing carbonyl group (1760 cm^{-1}), aromatic compounds (1412 cm^{-1}) and aliphatic esters (1120 cm^{-1}) are released. The peak at 2180 cm^{-1} with a shoulder at 2110 cm^{-1} is attributed to CO which occurs at 18.2 min. All of the peaks reach the maximal values which correspond to the maximal mass loss rate of PLA at 20.2 min. After 20.2 min, the spectra only leave a strong peaks at 1760 cm^{-1} and weak peaks at 1412 cm^{-1} and 1120 cm^{-1}.

Figure 11(b) shows the evolved gas-phase from the thermal decomposition of PLA/20AHP, which shows few differences from that of PLA. However, at 17.2 min, a new peak at 2320 cm^{-1} corresponds to the phosphine gas. This
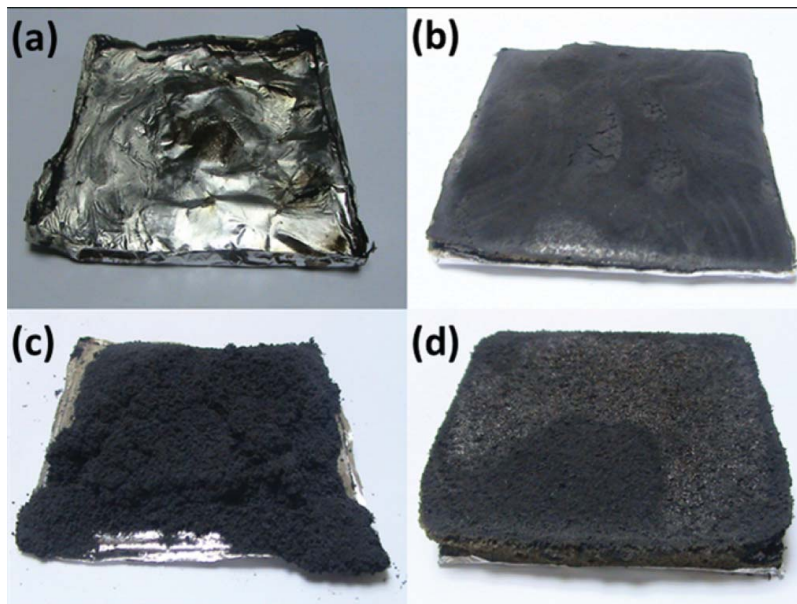
Fig. 9. Photos of studied samples after cone calorimeter test: (a) neat PLA; (b) PLA/20AHP; (c) PLA/20EG; (d) PLA/15AHP/5EG. (Color figure available online.)
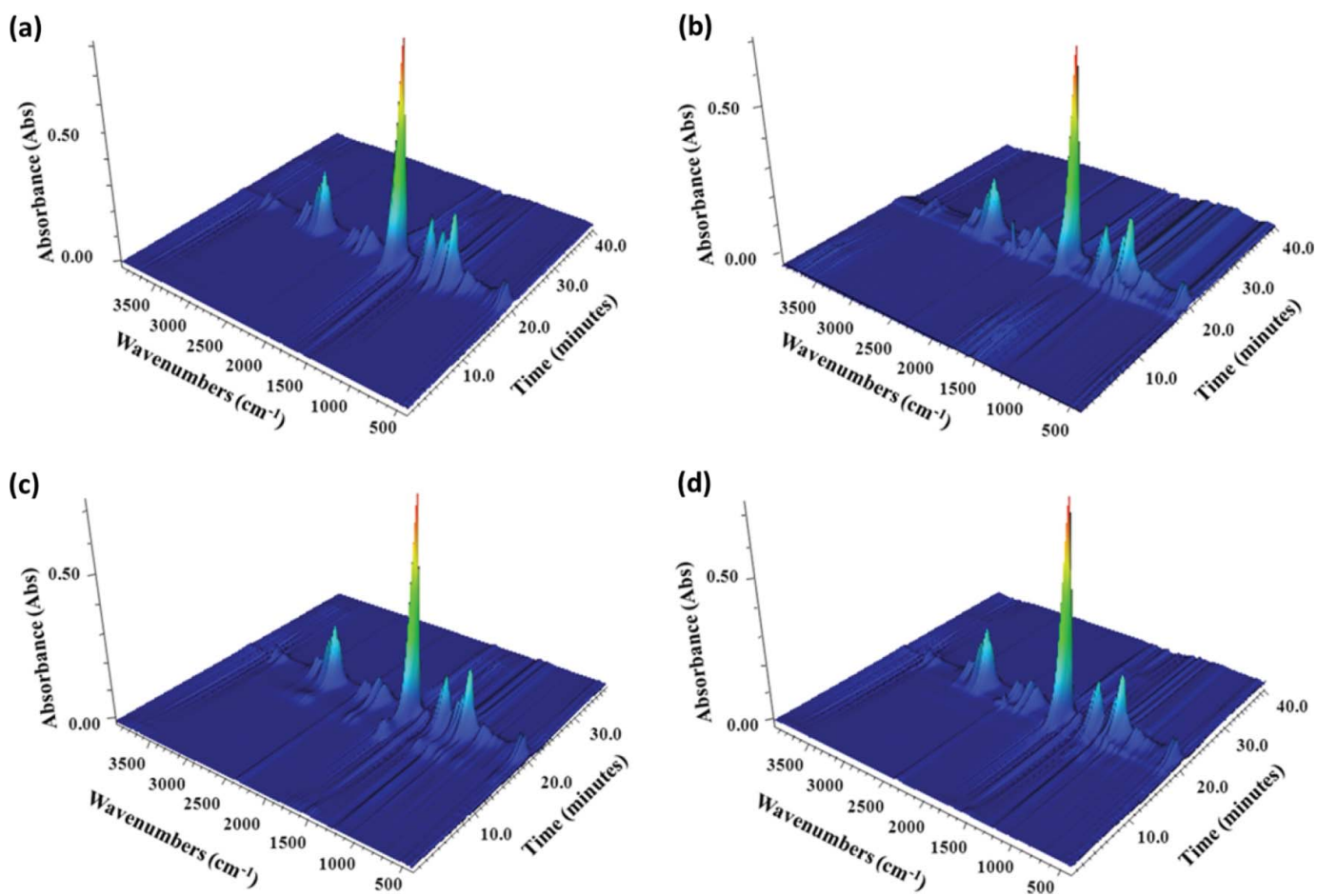

Fig. 10. 3D TG-FTIR spectra of gas phase in the thermal degradation of PLA and FR-PLA composites: (a) neat PLA; (b) PLA/20AHP; (c) PLA/20EG; (d) PLA/10AHP/10EG. (Color figure available online.)
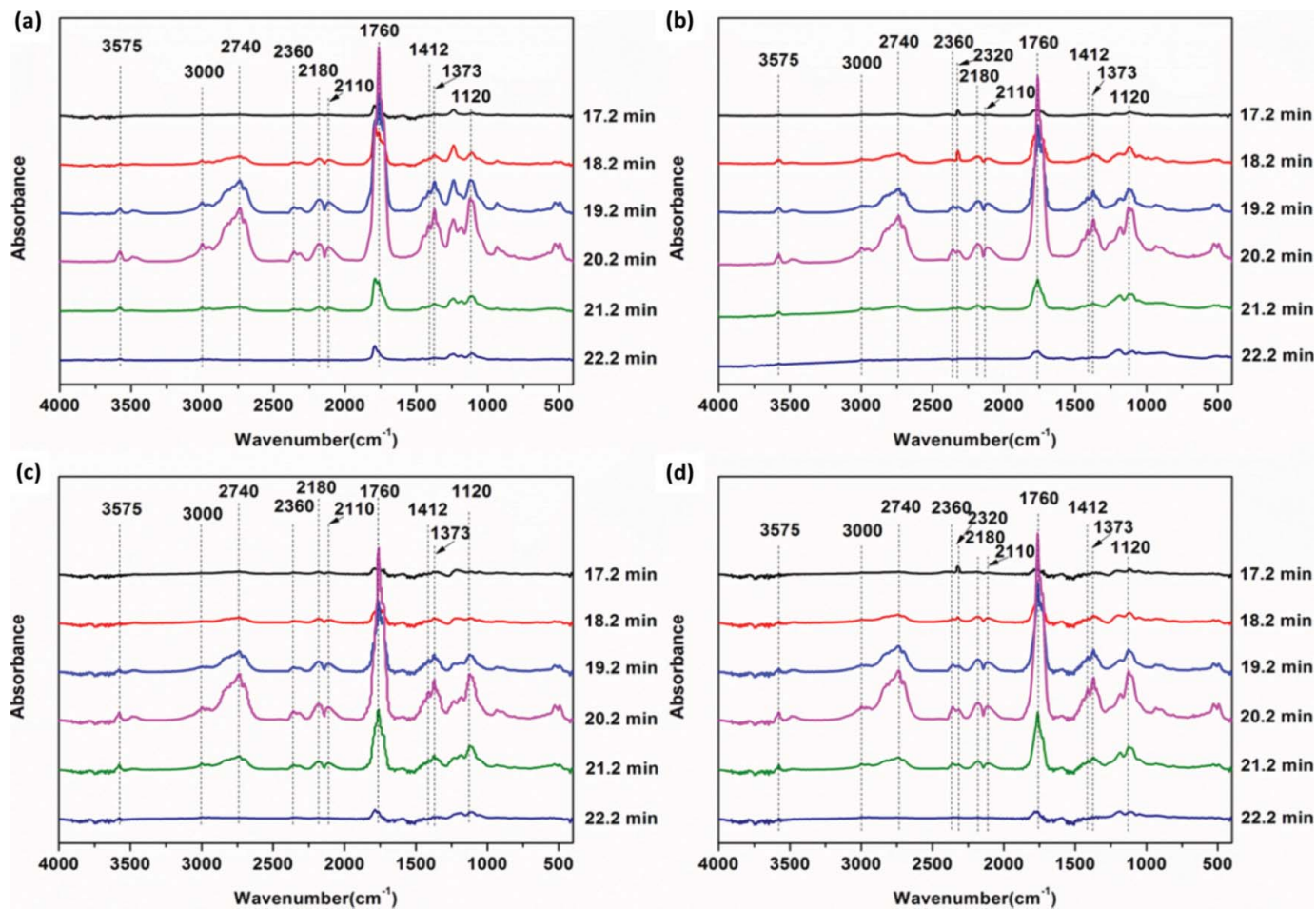
Fig. 11. FTIR spectra of volatilized products at various times during the thermal decomposition of PLA and FR-PLA composites: (a) PLA, (b) PLA/20AHP, (c) PLA/20EG, (d) PLA/10AHP/10EG. (Color figure available online.)

is consistent with the TG test, indicating the decomposition of AHP content.

Figure 11(c) shows the evolved gas-phase from the thermal decomposition of PLA/20EG. It is interesting to find that most of the characterized peaks at 21.2 min, which is different from pure PLA. This may come from that the expanded EG lamellar could increase the escape distance of the evolved gases.

Figure 11(d) shows the evolved gas-phase from the thermal decomposition of PLA/10AHP/10EG. It presents the similar features to Figure 11(b) and (c). In order to further understand the relationship between flame retardant additives and the product release rate, the absorbance of pyrolysis products for PLA and FR-PLA vs. time is revealed in Figure 12. Figure 12(a) illustrates the absorbance intensity of the total gases (Gram–Schmidt) for the two composites. The other seven figures show the absorbance intensity of water, hydrocarbons, CO_2, PH_3, CO, carbonyl groups and aromatic compounds, respectively. It can be found that the absorbance intensity of pyrolysis products of FR-PLA composites is much lower than that of pure PLA. This may come from the following reasons: for PLA/20AHP, the ad-

dition of AHP could form a compact inorganic layer, which can inhibit the escape of the gas products; for PLA/20EG, EG can expand and the lamellar structure can play as a micro-reactor for gas products; for PLA/10AHP/10EG, both of the above two effects exist in the composites. Furthermore, the addition of EG only result in a small peaks at 15 min, which is attributed to that the acid species (H_2SO_4, HNO_3) in the EG promote the degradation of PLA. It can be concluded that the addition of AHP and EG could reduce the gas products of PLA, and the combination of the two additives can reach a better effect.

3.7 The Analysis of Residue Char

The char residues of FR-PLA composites after cone calorimeter test were further investigated by SEM, as shown in Figure 13. The residue of PLA/20AHP (Fig. 13a) shows some holes on the surface and the holes may be caused by the impact of PH_3 during the decomposition of AHP. Compact char layer consisted of micron-sized particles is observed in Figure 13(b) at high magnification. In Figure 13(c), the char of PLA/20EG presents some
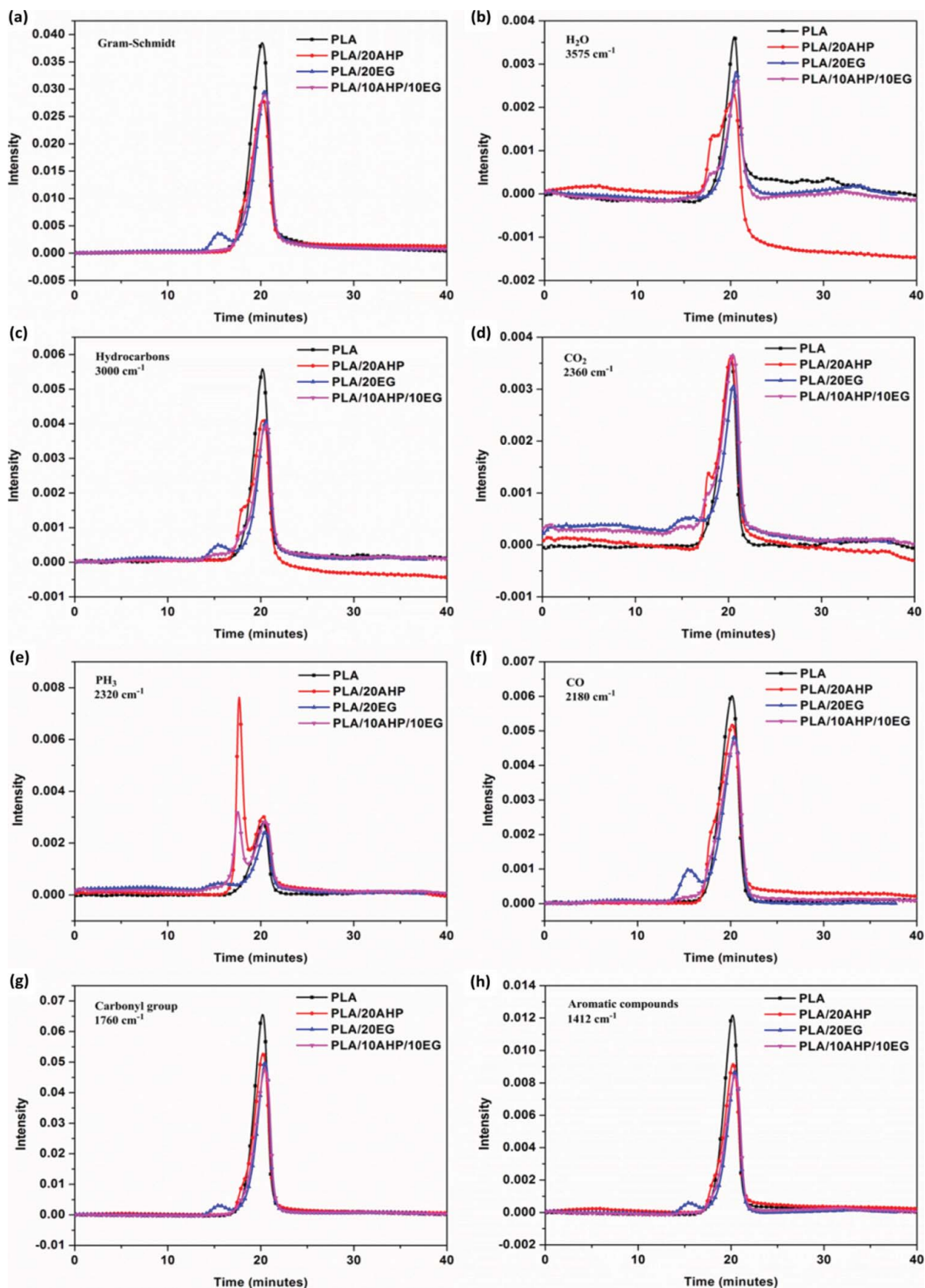
Fig. 12. Absorbance of pyrolysis products for PLA and FR-PLA composites vs. time: (a) Gram-Schmidt, (b) H_2O, (c) hydrocarbons, (d) CO_2, (e) PH_3, (f) CO, (g) carbonyl groups, (h) aromatic compounds. (Color figure available online.)
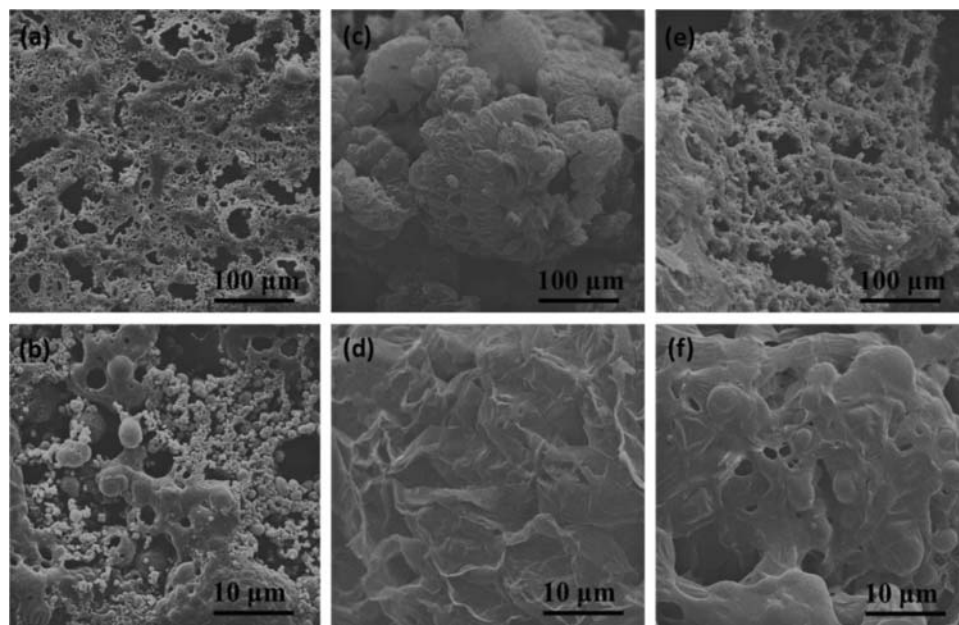
Fig. 13. SEM images of the char residue after cone calorimeter test: PLA/20AHP, (a, b); PLA/20EG, (c, d); PLA/15AHP/5EG, (e, f).

wormlike expanded graphite agglomerates on the surface, and the high magnification micrographs (Fig. 13d) indicates that EG particles of the burned composite have expanded many times. Figure 13(e) shows the low magnification of char morphology of PLA/15AHP/5EG, which displays some layered structures on the surface of char that may come from the decomposition of EG. In Figure 13(f), it is interesting to find that almost all the holes are covered, indicating that the combination of EG and AHP leads to the formation a compact and intumescent char layer.

In order to further investigate the improved flame retardancy, the residue char from cone calorimeter test were analyzed by FTIR and the corresponding spectra are shown in Figure 14. To the spectra of char residue of PLA/20EG, the peak at 3514 cm^{-1} is attributed to the absorbed water. The weak peaks at 2926 cm^{-1} and 2850 cm^{-1} correspond to symmetrical stretching and asymmetrical stretching of –CH2- group, indicating the addition of EG could prohibit the degradation of PLA chain. The peak at 1627 cm^{-1} indication the formation of C=C in the degradation
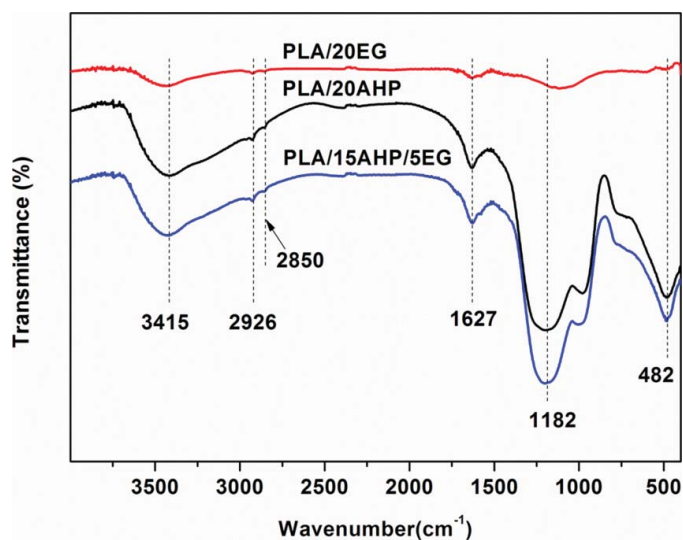

Fig. 14. FTIR spectra of char residues from FR-PLA composites after cone calorimeter test. (Color figure available online.)
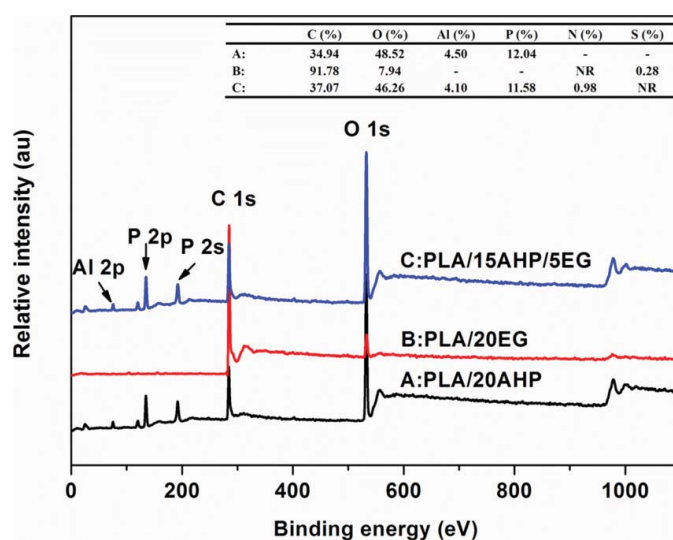

Fig. 15. XPS spectra of the char residue of FR-PLA composites after cone calorimeter test. (Color figure available online.)
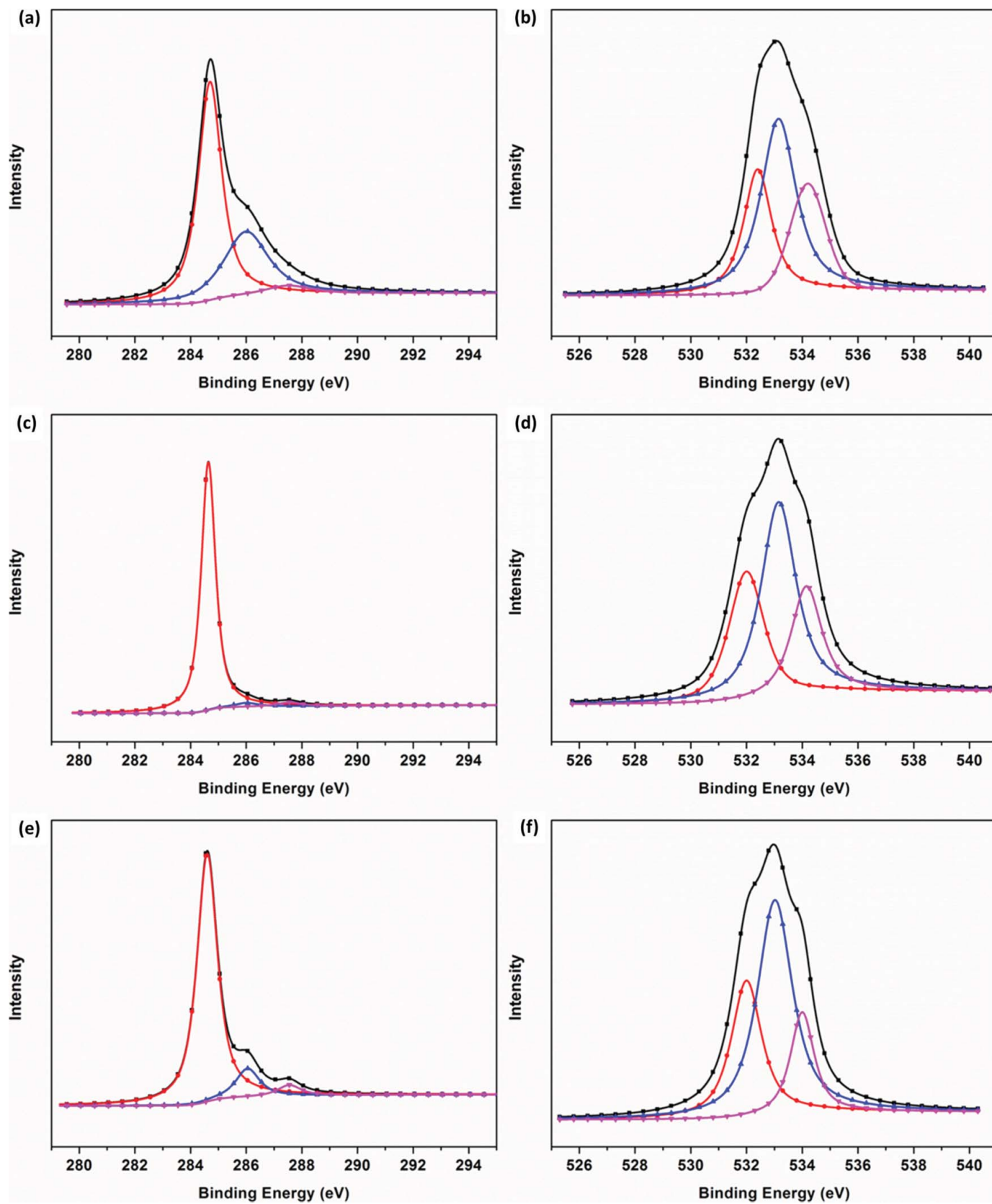
Fig. 16. C1s and O1s spectra of the char residue of FR-PLA composites: PLA/20AHP (a, C1s; b, O1s); PLA/20EG (c, C1s; d, O1s); PLA/15AHP/5EG (e, C1s; f, O1s). (Color figure available online.)
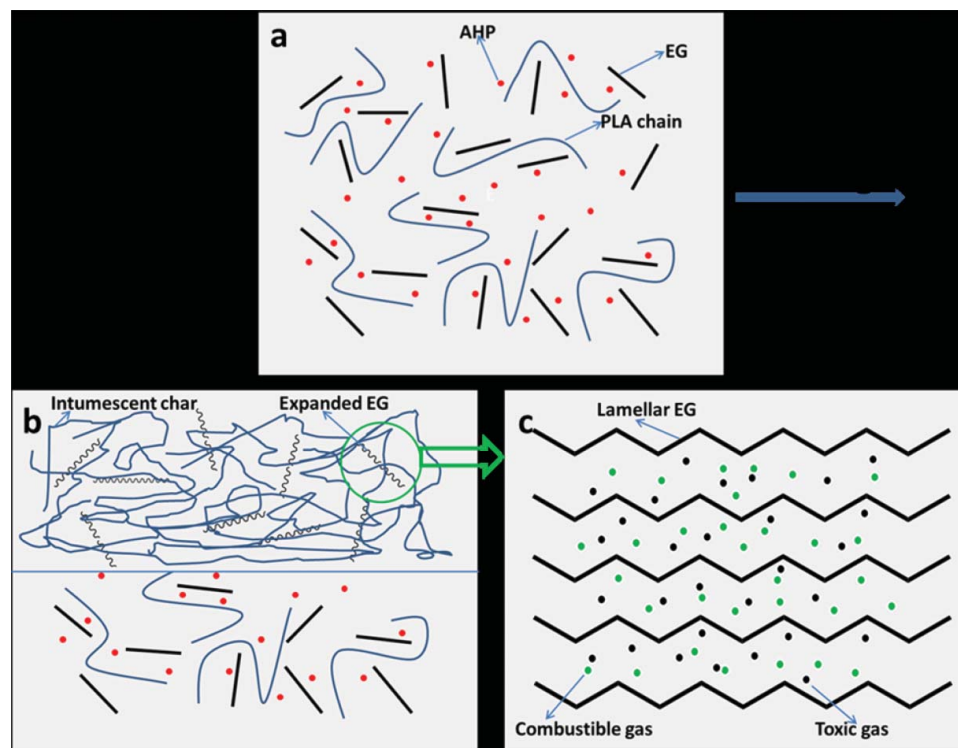
Fig. 17. The possible flame retardant mechanism of PLA/AHP/EG composites. (Color figure available online.)

process. To the spectra of char residue of PLA/20AHP and PLA/10AHP/10EG, the addition of AHP significantly increases the intensity of peak at 1627 cm^{-1}, indicating AHP could promote the formation of unsaturated structure. Furthermore, two new bonds at 1182 cm^{-1} and 482 cm^{-1} correspond to stretching vibration of PO$_2$ and Al-O bond stretch modes, indication the formation of Al$_4$(P$_2$O$_7$)$_3$ (36).

The chemical components of the residual char after cone calorimeter were also investigated by XPS, and the corresponding spectra are shown in Figure 15. It can be found that the addition of AHP significantly increase the carbon content in the residue char, this is because that the released PH$_3$ could be further oxidized in to phosphoric acid which can promote the carbonization of the composites. The residue char of PLA/20EG mainly contains carbon and oxygen, and also few sulfur elements which may come from EG. The combination of AHP and EG result in a slight increase of carbon element but decrease the element content of oxygen, sulfur and phosphorus. To further investigate the existing state of carbon and oxygen elements, the peaks were resolved using peak analysis software (XPSPEAK4.1). The corresponding spectra are shown in Figure16. The peak at 284.7 eV is attributed to C−H and C−C in aliphatic and aromatic species. The band at around 286.0 eV is assigned to C−O (ether and/or hydroxyl group and/or C−O−P in hydro-carbonated phosphate). Moreover, the peak at 287.5 eV is characteristics of carbonyl groups. It can be found that in the char residue of PLA/20AHP and PLA/15AHP/5EG, the carbon of-

ten in the state of C−C bond and C−O bond. And in the char residue of PLA/20EG the carbon element exist in the state of graphitic carbon (37). Three bonds are observed from the O1s spectra. The peak at 532.4 eV is attributed to =O in phosphate or carbonyl groups, and the peak at 533.2 eV is assigned to −O− in C−O−C, C−O−P and/or C−OH groups (38). The peak at 534.2 eV corresponds to chemisorbed oxygen and/or absorbed water (32).

3.8 Mechanism Consideration

On the basis on the above experimental datum, the possible mechanism of AHP with EG in PLA/AHP/EG composites systems was presented in Figure 17. AHP could thermal decomposed in the burning process and form three dimensional network structure. Meanwhile, PLA was dehydrogenated and oxidized and form C−OH group on the backbone. Then the crosslinking occurs among PLA/AHP system, resulting in the formation of a protective char layer on the surface of the materials (39). This char layer not only shields the polymer matrix from the external thermal radiation, but also holds back exterior oxygen and interior fuel, which resulted in improved flame retardancy of PLA/AHP composites. When EG was introduced into PLA/AHP flame retarded system, the synergism action of PLA/AHP/EG system was a complicated process. EG plays as an efficient intumescent agent as it acts as a carbonization compound. The EG particle rapidly expands and form vermicular structure which could further

prohibit the transportation of oxygen and fuel. Further-more, the space of vermicular structure could act as a "micro-reactor", which is approximately seemed as a closed room in which AHP or its decomposition products can adequately react with the decomposition products of PLA. The sufficient reaction significantly inhibits the combustible and toxic gas, result in an enhanced fire safety. Consequently, the flame retardancy is remarkably improved. At the same time, the results of the fire resistant tests all consist well with the mechanism.

4 Conclusions

Flame retarded PLA composites with AHP and EG were prepared by the melt blending method. The FR-PLA composites were investigated by TGA, LOI, UL-94, MCC, cone calorimeter testing TG-IR, FTIR, XPS and SEM. Both in the nitrogen and air conditions, the addition of AHP and EG dramatically increased the char yield. The LOI value of the PLA/10AHP/10EG could be increased to 34%, which is higher than PLA/20AHP whose LOI is 28.5%. The cone calorimeter result of PLA/AHP/EG composites showed low heat release rate, total heat release and high amounts of char residues after combustion. TG-IR result revealed that the addition of AHP and EG could significantly decrease the yield of gas-phase products. All results indicate that EG has a significant synergistic effect, which occurs when EG and AHP are both present in FR-PLA composites. Based on the above data, the possible flame retardant mechanism of PLA/AHP/EG composite was also discussed.

Acknowledgments

References

1. Li, S.M., Ren, J., Yuan, H., Yu, T. and Yuan, W.Z. (2010) *Polym. Int.*, 59, 242–248.
2. Yu, T., Ren, J., Li, S.M., Yuan, H. and Li, Y. (2010) Composites. *Part A*, 41, 499–505.
3. Rasal, R.M., Janorkar, A.V. and Hirt, D.E. (2010) *Prog. Polym. Sci.*, 35, 338–356.
4. Zhang, J.F. and Sun, X.Z. (2004) *Biomacromolecules*, 5, 1446–1451.
5. Li, B.H. and Yang, M.C. (2006) *Polym. Adv. Technol.*, 17, 439–443.
6. Garlotta, D. (2002) *J. Polym. Environ.*, 9, 63–84.
7. Carrasco, F., Pagès, P., Gámez-Pérez, J., Santana, O.O. and Maspoch, M.L. (2010) *Polym. Degrad. Stab.*, 95, 116–125.
8. Hata, Isamu. *J. P. Pat.* No. 2006335929.
9. Sunagawa, Takenobu. *J. P. Pat.* No. 2006193561.
10. Oda, Tatsuaki. *J. P. Pat.* No. 2006077162.
11. Ihara, Toshiaki; Tanaka, Masaki; Matsumura, Kazuyuki. *E. P. Pat.* No. 1674551.
12. Yamashita, Takehiko; Takeda, Kunihiko; Tani, Yoshiyuki; Hisazumi, Takao. *PCT Pat*. Appl. WO 2005028558.
13. Chin, Hui. *J. P. Pat.* No. 2004190025.
14. Yang, W., Song, L., Hu, Y., Lu, H.D and Yuen, Richard K.K. (2011) *Composites Part B*, 42, 1057–1065.
15. Yang, W., Hu, Y., Tai, Q. L., Lu, H. D., Song, L. and Yuen, Richard K.K. (2011) *Composites Part A*, 42, 794–800.
16. Braun, U., Schartel, B., M. Fichera, A. and Jäger, C. (2007) *Polym. Degrad. Stab.*, 92, 1528–1545.
17. Li, Y.C. and Chen, G.H. (2007) *Polym. Eng. Sci.*, 47, 882–888.
18. Goyal, R.K., Jagadale, P.A. and Mulik, U.P. (2009) *J. Appl. Polym. Sci.*, 111, 2071–2077.
19. George, J.J. and Bhowmick, A.K. (2008) *J. Mater. Sci.*, 43, 702–708.
20. Wang, W.P., Liu, Y., Li, X.X. and You,Y.Z. (2006) *J. Appl. Polym. Sci.*, 100, 1427–1431.
21. Zhang, X.L., Shen, L., Xia, X., Wang, H.T. and Du, Q.G. (2008) *Mater. Chem. Phys.*, 111, 368–374.
22. Bian, X.C., Tang, J.H., Li, Z.M., Lu, Z.Y. and Lu, A. (2007) *J. Appl. Polym. Sci.*, 104, 3347–3355.
23. Qu, B.J. and Xie, R.C. (2003) *Polym. Int.*, 52, 1415–1422.
24. Tsai, K.C., Kuan, H.C., Chou, H.W., Kuan, C.F., Chen, C.H. and Chiang, C.L. (2011) *J. Polym. Res.*, 18, 483–488.
25. Ye, L., Meng, X.Y., Liu, X.M., Tang, J.H. and Li, Z.M. (2009) *J. Appl. Polym. Sci.*, 111, 2372–2380.
26. Li, Z.Z. and Qu, B.J. (2003) *Polym. Degrad. Stab.*, 81, 401–408.
27. Meng, X.Y., Ye, L., Zhang, X.G., Tang, P.M., Tang, J.H., Ji, X. and Li, Z.M. (2009) *J. Appl. Polym. Sci.*, 114, 853–863.
28. Murariu, M., Dechief, A.L., Bonnaud, L., Paint, Y., Gallos, A., Fontaine, G., Bourbigot, S. and Dubois, P. (2010) *Polym. Degrad. Stab.*, 95, 889–900.
29. Kandare, E., Chukwudolue, C.and Kandola, B.K. (2010) *Fire Mater.*, 34, 21–38.
30. Lyon, R.E., Walters, R.N. and Stoliarov, S.I. (2007) *Polym. Eng. Sci.*, 47, 1501–1510.
31. Costantino, U., Gallipoli, A., Nocchetti, M., Camino, G., Bellucci, F. and Frache, A. (2005) *Polym. Degrad. Stab.*, 90, 586–590.
32. Wang, X., Hu, Y., Song, L., Xuan, S.Y., Xing, W.Y., Bai, Z.M. and Lu, H.D. (2011) Ind. *Eng. Chem. Res.*, 50, 713–720.
33. Wu, K., Hu, Y., Song, L., Lu, H. D., Wang, Z.Z. (2009) Ind. *Eng. Chem. Res.*, 48, 3150–3157.
34. Braun, U., Balabanovich, A.I., Schartel, B. (2006) *Polymer*, 47, 8495–8508.
35. Wu, K., Song, L., Hu, Y., Lu, H. D., Kandola, B.K., Kandare, E. (2009) *Prog. Org. Coat.*, 65, 490–497.
36. Yoshida, Y., Inoue, K., Kyritsakas, N., Kurmoo, M. (2009) *Inorga. Chim. Acta.*, 362, 1428–1434.
37. Krawczyk, P. *Chem. Eng. J.*, (2011) 172, 1096–1102.
38. Bourbigot, S., Le Bras, M., Delobel, R., Gengembre, L. (1997) *Appl. Surf. Sci.*, 120, 15–29.
39. Zhang, P., Hu, Y., Song, L., Ni, J.X., Xing, W.Y., Wang, J. (2010) *Sol. Energy Mater. Sol. Cells*, 94, 360–365.